

Article

# Ni-CNT Chemical Sensor for SF<sub>6</sub> Decomposition Components Detection: A Combined Experimental and Theoretical Study

Yingang Gui <sup>1,\*</sup>, Xiaoxing Zhang <sup>3,\*</sup>, Peigeng Lv <sup>2</sup>, Shan Wang <sup>2</sup>, Chao Tang <sup>1</sup>  
and Qu Zhou <sup>1</sup>

<sup>1</sup> College of Engineering and Technology, Southwest University, Chongqing 400715, China; tangchao\_1981@163.com (C.T.); zhouqu@swu.edu.cn (Q.Z.)

<sup>2</sup> State Grid Chongqing Shiqu Power Supply Company, Chongqing 400015, China; 13983772950@139.com (P.L.); shan102330@msn.com (S.W.)

<sup>3</sup> School of Electrical Engineering, Wuhan University, Wuhan 430072, China

\* Correspondence: yinganggui@swu.edu.cn (Y.G.); xiaoxing.zhang@outlook.com (X.Z.)

Received: 11 September 2018; Accepted: 12 October 2018; Published: 16 October 2018



**Abstract:** SF<sub>6</sub> decomposition components detection is a key technology to evaluate and diagnose the insulation status of SF<sub>6</sub>-insulated equipment online, especially when insulation defects-induced discharge occurs in equipment. In order to detect the type and concentration of SF<sub>6</sub> decomposition components, a Ni-modified carbon nanotube (Ni-CNT) gas sensor has been prepared to analyze its gas sensitivity and selectivity to SF<sub>6</sub> decomposition components based on an experimental and density functional theory (DFT) theoretical study. Experimental results show that a Ni-CNT gas sensor presents an outstanding gas sensing property according to the significant change of conductivity during the gas molecule adsorption. The conductivity increases in the following order: H<sub>2</sub>S > SOF<sub>2</sub> > SO<sub>2</sub> > SO<sub>2</sub>F<sub>2</sub>. The limit of detection of the Ni-CNT gas sensor reaches 1 ppm. In addition, the excellent recovery property of the Ni-CNT gas sensor makes it easy to be widely used. A DFT theoretical study was applied to analyze the influence mechanism of Ni modification on SF<sub>6</sub> decomposition components detection. In summary, the Ni-CNT gas sensor prepared in this study can be an effective way to evaluate and diagnose the insulation status of SF<sub>6</sub>-insulated equipment online.

**Keywords:** SF<sub>6</sub> decomposition components; carbon nanotube sensor; Ni modification; adsorption; DFT calculations

## 1. Introduction

Due to the strong insulation strength and electronegativity of SF<sub>6</sub> gas, it has been widely used as filling gas in insulated equipment, such as SF<sub>6</sub>-insulated high-voltage switchgear (GIS), SF<sub>6</sub>-insulated transmission lines (GIL), and SF<sub>6</sub>-insulated circuit breakers (GCB) [1–3]. However, insulation defects inevitably occur in SF<sub>6</sub>-insulated equipment, which induces SF<sub>6</sub> to decompose into various decomposition components: SO<sub>2</sub>, H<sub>2</sub>S, SOF<sub>2</sub>, and SO<sub>2</sub>F<sub>2</sub> under electric discharge [4–7]. In addition, the existence of insulation defects and SF<sub>6</sub> decomposition dramatically reduce the insulation strength of SF<sub>6</sub>-insulated equipment [8]. A lot of methods have been studied to detect the insulation defects, including the ultra-high frequency method (UHF) [9,10], the transient earth voltage method (TEV) [11], the ultrasonic method [12], the gas chromatographic method [13], and the gas sensor detection method [14]. However, UHF, TEV, and the ultrasonic method are easily affected by interference signals, and the gas chromatographic method is an offline detection method. Because of the non-contact, high accuracy, and low detection limit features of gas sensors, the gas sensor detection

method has been an effective way to realize the online detection of SF<sub>6</sub>-insulated equipment based on SF<sub>6</sub> decomposition components detection [15,16].

One dimensional carbon nanotube (CNT) material has attracted extensive study due to its outstanding characteristics [17,18], such as large specific surface area and good electrical properties. It is demonstrated that CNTs shows excellent gas sensing performance to gases [19,20], making it an effective detection method used in environmental, industrial, and military fields [21,22]. Li et al. fabricated single-wall carbon nanotube (SWNT) based gas sensors on interdigitated gold electrodes; its detection limit reaches 44 ppb for NO<sub>2</sub> and 262 ppb for nitrotoluene at room temperature [19]. Chopra et al. reported that multi-wall carbon nanotube (MWCNT) and polymer composites exhibited excellent sensitivity and selectivity to NH<sub>3</sub> and NO<sub>2</sub> at room temperature [23]. Surface modification based on metal particles can greatly improve the gas sensitivity and selectivity of CNTs. Penza et al. verified that the functionalization of Pt and Pd nanoclusters on the MWCNT surface significantly improved its detection limit to sub-ppm level upon NO<sub>2</sub>, H<sub>2</sub>S, NH<sub>3</sub>, and CO detection [24]. Although the development of CNT gas sensors has made a remarkable improvement in common gas detection, there are few reports about its application in the field of SF<sub>6</sub> decomposition components detection.

Here, Nickel functionalized CNTs (Ni-CNTs) are adopted as the gas sensing material to detect the characteristic SF<sub>6</sub> decomposition components: SO<sub>2</sub>, H<sub>2</sub>S, SOF<sub>2</sub> and SO<sub>2</sub>F<sub>2</sub>. Experimentally, the Ni-CNT gas sensor is prepared by the drop-casting method, which significantly reduces the preparation cost and benefits for industrial-scale production. In addition, the gas sensing mechanism of Ni-CNTs to the characteristic SF<sub>6</sub> decomposition components is studied by density functional theory (DFT) calculation. We conclude that the Ni-CNT gas sensor can be an effective way to detect the insulation defects and diagnose the running status of SF<sub>6</sub>-insulated equipment online.

## 2. Material and Methods

### 2.1. Synthesis of Ni-CNT Gas Sensor

Ni-CNTs (inner diameter: 5–10 nm, external diameter: 10–20 nm, and length: 10–30 μm) were bought from Aladdin Reagent Corporation (Shanghai, China). Figure 1a shows the interdigitated Cu electrodes; Cu electrodes (thickness: 30 μm, gap: 0.2 mm) were fabricated on epoxy resin as a substrate of the Ni-CNT gas sensor. Ni-CNTs were dispersed in dimethylformamide (DMF) to form a solution of 0.025 mg/mL by the following steps: soak 6 h, then ultrasonic treat 2 h. The solution was sprayed onto the surface of the Cu electrodes at 80 °C to accelerate the evaporation of DMF. As shown in Figure 1b, Ni-CNTs evenly distribute on the surface of the Cu electrodes, which benefits the gas molecule adsorption and desorption process.

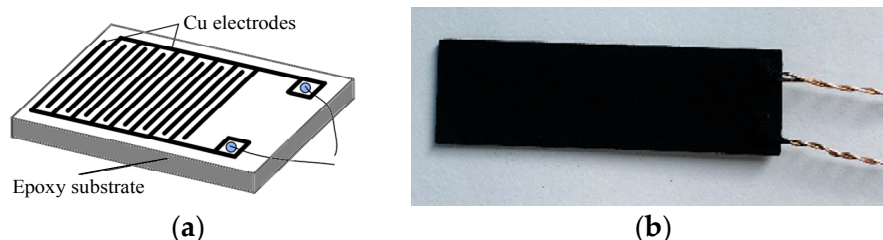


**Figure 1.** (a) Interdigitated Cu electrodes, (b) the prepared Ni-modified carbon nanotube (Ni-CNT) gas sensor.

### 2.2. Material Characterization and Gas Sensing Measurement

Transmission electron microscopy (TEM) was tested by FEI Tecnai G2 F20 S-TWIN at 200 kV. The gas-sensing detection system was composed of standard gases (SO<sub>2</sub>, H<sub>2</sub>S, SOF<sub>2</sub>, and SO<sub>2</sub>F<sub>2</sub>), the gas distribution system, the gas sensing chamber, and an electrochemical workstation. The concentration

of standard gases was 400 ppm with N<sub>2</sub> as the background gas. The standard gases were diluted to different concentrations: 1, 10, 50, 100, 200, 300, and 400 ppm by the gas distribution system. Then, the diluted gases were led to the closed gas chamber. The resistance of the Ni-CNT gas sensor was measured by the electrochemical workstation at room temperature and ambient pressure. The gas response (*GR*) was defined by Equation (1). In which, *R<sub>i</sub>* is the initial electric resistance of the Ni-CNT gas sensor in dry synthesis air and *R<sub>f</sub>* is the resistance of the sensor in SF<sub>6</sub> decomposition components' atmosphere. In addition, the sensitivity (*S*) of the Ni-CNT gas sensor was defined by Equation (2), where *C<sub>T</sub>* was the concentration of tested gas.

$$GR = \frac{R_f - R_i}{R_i} \times 100\% \quad (1)$$

$$S = \frac{G.R}{C_T} \times 100\% \quad (2)$$

### 2.3. DFT Calculation

The DFT calculations were performed using Dmol<sup>3</sup> package of materials studio. The structure of (8, 0) Ni-CNTs was built by substituting a carbon atom by one Ni atom. In addition, a 20 × 20 × 8.5 Å periodic-boundary supercell was built to avoid the interference of adjacent cells. Then, the optimized adsorption structures of SO<sub>2</sub>, H<sub>2</sub>S, SOF<sub>2</sub>, and SO<sub>2</sub>F<sub>2</sub> on the surface of Ni-CNTs were calculated with different initial gas positions. The Perdew–Burke–Ernzerhof (PBE) function generalized gradient approximation was adopted to treat the exchange-correlation potential. The convergence criterion for energy and force was set at 10<sup>−5</sup> Ha and 2 × 10<sup>−3</sup> Ha/Å, respectively. The Brillouin zone was sampled with 1 × 1 × 2 Monkhorst–Pack mesh. The adsorption energy (*E<sub>ads</sub>*) of the molecules adsorbed on Ni-CNTs was defined by the following Equation (3):

$$E_{ads} = E_{gas/surf} - E_{gas} - E_{surf} \quad (3)$$

where *E<sub>gas/surf</sub>* was the energy of gas adsorbed CNTs, *E<sub>surf</sub>* and *E<sub>gas</sub>* were the energy of isolated Ni-CNTs and molecules of SF<sub>6</sub> decomposition components.

The electron density distribution was obtained by Mulliken population analysis. The charge transfer (*Q<sub>t</sub>*) in the adsorption process was defined by Equation (4), where *Q<sub>iso</sub>* and *Q<sub>ads</sub>* were the respective total charge of gas molecules before and after adsorption.

$$Q_t = Q_{ads} - Q_{iso} \quad (4)$$

## 3. Results and Discussion

### 3.1. Preparation and Gas Sensing Property of Ni-CNT Gas Sensor

As per the formation mechanism of Ni-CNTs shown in Figure 2a, it is important to make sure that Ni particles evenly decorate onto the outside wall of intrinsic CNTs, which plays a key role to the gas-sensing properties of the prepared Ni-CNT gas sensor. As per the typical TEM images shown in Figure 2b–d with different magnifications, Ni-CNTs evenly disperse on the surface of the prepared gas sensor. Hence, there will be large, hollow structures for gas diffusion among the Ni-CNTs, which not only increase the adsorption capacity, but reduce the adsorption and desorption time. Ni nanoparticles mainly distribute on the outside wall of CNTs due to the long length and closed structure of CNTs (about 30 μm). The small diameter of Ni-CNTs (about 20 nm) signifies large curvature and high surface activity. Besides, the surface defects that existed on the surface of CNTs provide the adsorption sites for gas molecules. As a result, Ni nanoparticles evenly decorate on the surface of CNTs with their size distinctly smaller than the diameter of CNTs. Ni nanoparticles act as the active sites for gas molecule adsorption, which effectively enhances the gas-sensing properties of CNT-based sensors.

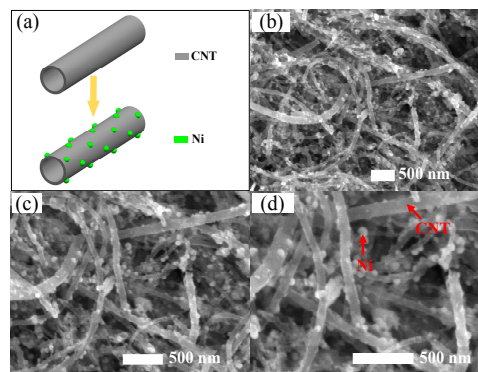


**Figure 2.** (a) The formation mechanism of Ni-CNTs, (b–d) structure characterization of Ni-CNTs.

Considering the concentration range of  $\text{SF}_6$  decomposition components generated in  $\text{SF}_6$ -insulated equipment reported in previous studies [4,25], a series of  $\text{SF}_6$  decomposition components concentrations, 1, 10, 50, 100, 200, 300, and 400 ppm, were prepared to analyze the gas-sensing performance of the Ni-CNT gas sensor. As shown in Figure 3, the resistance of the gas sensor significantly reduces when it contacts  $\text{SF}_6$  decomposition components [26–29]. The Ni-CNT gas sensor presents a large gas response to  $\text{SF}_6$  decomposition components at room temperature and ambient pressure due to the catalytic property of evenly distributed Ni nanoparticles. Furthermore, the CNT sensor presents a fast gas response because of the large gas diffusion channel among Ni-CNTs, which also implies a fast gas-sensing recovery speed. The resistance rapidly reduces when the sensor just contacts the  $\text{SF}_6$  decomposition components, because the gas molecules quickly interact with the gas-sensing material on the surface of the Ni-CNT gas sensor. Meanwhile, the reduction speed gradually decreased as the gas diffusion rate sharply reduced with diffusion depth in the sensor film.

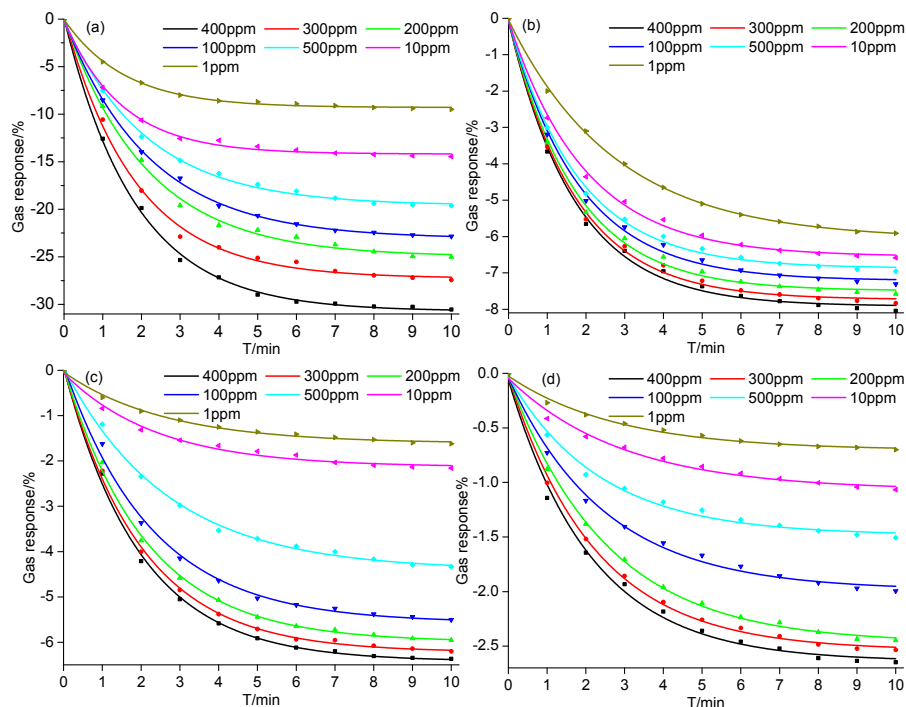


**Figure 3.** Gas response of the Ni-CNT gas sensor to different concentrations of  $\text{SF}_6$  decomposition components: (a)  $\text{H}_2\text{S}$ , (b)  $\text{SOF}_2$ , (c)  $\text{SO}_2$ , and (d)  $\text{SO}_2\text{F}_2$  at room temperature and ambient temperature.

As shown in Figure 3, it takes about 10 min for the gas response to reach a steady state. The variation of gas response is greatly influenced by the concentration of  $\text{SF}_6$  decomposition

components. For instance, the difference of gas response as the gas concentration increases from 300 to 400 ppm is smaller than that of 200 to 300 ppm. Comparing the value of gas responses shown in Figure 3a–d under the same gas concentration, the variation of gas responses is placed in the following order:  $\text{H}_2\text{S} > \text{SOF}_2 > \text{SO}_2 > \text{SO}_2\text{F}_2$ . The largest value of gas response to  $\text{H}_2\text{S}$  is  $-30.54\%$  at the concentration of 400 ppm, and the value of the gas response still reached  $-9.50\%$  at the lowest concentration (1 ppm) as shown in Figure 3a. The high gas response mainly comes from the strong interaction between Ni-CNTs and  $\text{H}_2\text{S}$  molecules at the Ni atom functionalized sites, which contributes to the detection of the  $\text{H}_2\text{S}$  component up to sub-ppm level. According to Figure 3b, the gas response of the Ni-CNT gas sensor to  $\text{SOF}_2$  changes a little under different gas concentrations. The gas responses at 400 ppm and 1 ppm are  $-8.04\%$  and  $-5.91\%$ , respectively. On the contrary, different concentrations of  $\text{SO}_2$  leads to a significant change of gas response, as shown in Figure 3c. The value of gas response increases from  $-1.62\%$  (1 ppm) to  $-6.37\%$  (400 ppm). Although Ni atom functionalization on the Ni-CNT surface enhances its adsorption to  $\text{SO}_2\text{F}_2$ , the Ni-CNT gas sensor was still not sensitive to  $\text{SO}_2\text{F}_2$ . As shown in Figure 3d, the gas responses to  $\text{SO}_2\text{F}_2$  are  $-2.65\%$  and  $-0.7\%$  at 400 ppm and 1 ppm, respectively. In summary, the Ni-CNT gas sensor shows a high gas response to  $\text{SF}_6$  decomposition components, and its high gas-sensing selectivity can be used to identify the gas types of  $\text{SF}_6$  decomposition components produced in  $\text{SF}_6$ -insulated equipment, making it suitable to detect the insulation defects and diagnose the running status of  $\text{SF}_6$  insulated equipment online.

Table 1 shows the comparison of the limit of detection (LOD) for different sensors to  $\text{SF}_6$  decomposition components reported in recent studies, including the most studied gas-sensing material: CNTs, graphene, and  $\text{TiO}_2$  nanotubes. In this study, the highest gas response of the Ni-CNT sensor studied in this work reaches  $-9.5\%$  upon 1 ppm  $\text{H}_2\text{S}$  measurement, which was slightly higher than that of reported CNT-based gas sensors. Meanwhile, a  $\text{TiO}_2$ -based gas sensor usually needs a high working temperature to receive a high gas response to  $\text{SF}_6$  decomposition components. It was reported that the LOD of Au-Graphene was only 50 ppm with a gas response of  $18.75\%$  to  $\text{H}_2\text{S}$  [28]. Therefore, the Ni-CNT sensor obviously presents advantages in high gas response and low working temperature.

**Table 1.** The limit of detection (LOD) of different gas sensors to  $\text{SF}_6$  decomposition components. RT represents room temperature. CNTs: carbon nanotubes.

Sensor	LOD (ppm)	T (°C)	Gas	Reference
Ni-CNTs	1	RT	$\text{H}_2\text{S}$	This work
Sieve/CNTs	10	RT	$\text{H}_2\text{S}$	Zhang et al. [30]
Pd-CNTs	50	RT	$\text{H}_2\text{S}$	Star et al. [31]
Pt- $\text{TiO}_2$ NTs	25	160	$\text{SO}_2$	Jing et al. [32]
Au-Graphene	50	RT	$\text{H}_2\text{S}$	Yu et al. [28]

To demonstrate the reusability of the prepared Ni-CNT gas sensor, we have done multiple measurements to obtain its response and recovery properties to different types of  $\text{SF}_6$  decomposition components at the same concentration (400 ppm). As shown in Figure 4, the flow rate of  $\text{SF}_6$  decomposition components is 100 sccm during the gas-sensing process, and the  $\text{N}_2$  flow is used in the recovery process with a flow rate of 200 sccm. In addition, the illumination of UV light is applied to enhance the recovery process as it greatly increases the molecular vibration of  $\text{SF}_6$  decomposition components. Gas-in and  $\text{N}_2 + \text{UV}$  represent the flow of  $\text{SF}_6$  decomposition components ( $\text{SO}_2$ ,  $\text{H}_2\text{S}$ ,  $\text{SOF}_2$ , and  $\text{SO}_2\text{F}_2$ ) and the flow of pure  $\text{N}_2$  flow with UV illumination, respectively. Simultaneously,  $\text{N}_2$  flow transfers the desorbed gas from the surface of Ni-CNTs and avoids re-adsorption. The Ni-CNT gas sensor still keeps a good gas response to  $\text{SO}_2$ ,  $\text{H}_2\text{S}$ ,  $\text{SOF}_2$ , and  $\text{SO}_2\text{F}_2$  after multiple gas adsorption and desorption detections, as the gas response changes little with measurement times. The value of gas response reduces from initially  $-30.54\%$  to  $-28.13\%$  upon  $\text{H}_2\text{S}$  detection. In addition, the change of gas response to  $\text{SOF}_2$ ,  $\text{SO}_2$ , and  $\text{SO}_2\text{F}_2$  was  $0.55\%$  (from  $-8.04\%$  to  $-7.49\%$ ),  $0.69\%$  (from  $-6.37\%$  to

5.68%), and 0.31% (from  $-2.65\%$  to  $-2.34\%$ ) after three lots of measurements, which is much less than the change of gas response to  $\text{H}_2\text{S}$ .

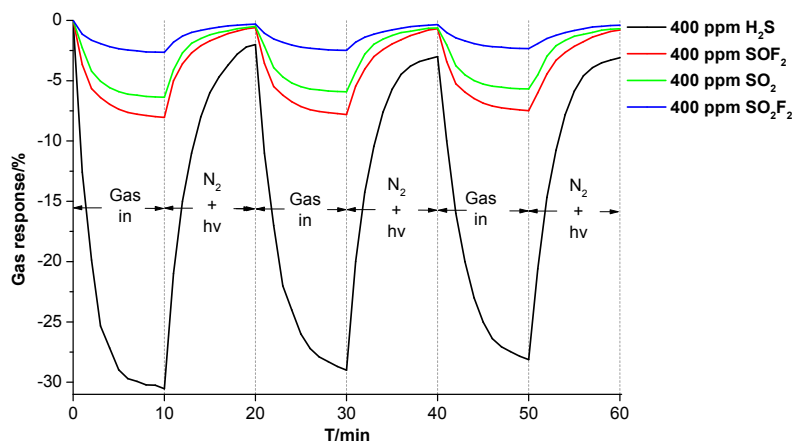


**Figure 4.** The gas response and recovery properties of the Ni-CNT gas sensor to  $\text{SF}_6$  decomposition components.

Figure 5a shows the change of gas response with the increase of concentration of  $\text{SF}_6$  decomposition components. Upon  $\text{H}_2\text{S}$  and  $\text{SOF}_2$  detection, the gas response sharply enhances when gas concentration increases from 1 to 50 ppm, and then tends to linearly increase under high gas concentration of detected gases, from 50 to 400 ppm. This also demonstrates that the Ni-CNT sensor is sensitive to  $\text{H}_2\text{S}$  and  $\text{SOF}_2$ . Upon  $\text{SO}_2$  and  $\text{SO}_2\text{F}_2$  detection, the increase of the gas response shows an exponential growth trend. Figure 5b shows the change of sensitivity to  $\text{SF}_6$  decomposition components; the sensitivity presents an exponential attenuation from 1 to 400 ppm, because it tends to be saturated at a high gas concentration. The attenuation speed is listed in the following order:  $\text{H}_2\text{S} > \text{SOF}_2 > \text{SO}_2 > \text{SO}_2\text{F}_2$  at the same gas concentration.

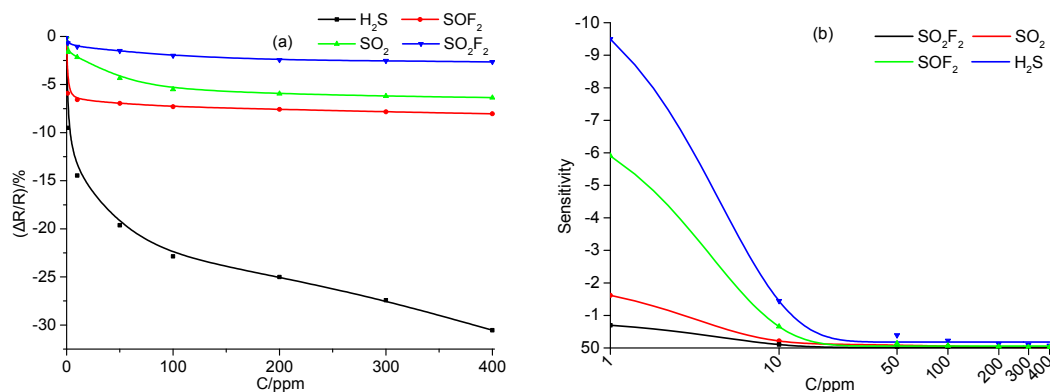


**Figure 5.** (a) The change of gas response, and (b) the change of sensitivity with the increase of concentration of  $\text{SF}_6$  decomposition components.

### 3.2. DFT Study of the Ni-CNT Gas Sensor

DFT study is used to analyze the adsorption properties of Ni-CNTs to  $\text{SF}_6$  decomposition components:  $\text{SO}_2$ ,  $\text{H}_2\text{S}$ ,  $\text{SOF}_2$ , and  $\text{SO}_2\text{F}_2$ . As Ni nanoparticles modified on the CNT surface always exist as clusters, single and double Ni atom-doped CNT structures are built to reflect the influence of Ni nanoparticles, represented by 1Ni-CNTs and 2Ni-CNTs. Figure 6 and Table 2 show the most stable adsorption structures and corresponding data for one gas molecule adsorption on Ni-CNTs. It is found that all the gas molecules tend to adsorb around Ni atoms due to its high adsorption activity.  $\text{SO}_2$ ,  $\text{H}_2\text{S}$ , and  $\text{SOF}_2$  interact with Ni-CNTs with physisorption. Due to the polyvalent properties of the

sulfur atom, the chemisorption between  $\text{SO}_2\text{F}_2$  and the Ni-CNT surface leads to the structure break of  $\text{SO}_2\text{F}_2$  in the adsorption process, reducing the reusability of the CNT gas sensor as it impedes the gas molecule desorption. The  $\text{H}_2\text{S}$  molecule interacts with Ni-CNTs by sulfur atoms. The nearest adsorption distance for  $\text{H}_2\text{S}$  reduces from 2.33 Å to 2.15 Å when the doped Ni atoms increase from single to double.  $\text{SO}_2$  and  $\text{SOF}_2$  molecules interact with Ni-CNTs by oxygen atoms rather than sulfur atoms because the sulfur atom has already built a strong covalent bond with two oxygen atoms or two fluorine atoms. The nearest adsorption distance for  $\text{SO}_2$  and  $\text{SOF}_2$  on 2Ni-CNTs are 1.88 Å and 1.94 Å, respectively. The nearest distance from the  $\text{SO}_2\text{F}$  that breaks from  $\text{SO}_2\text{F}_2$  to Ni-CNTs is 1.86 Å on 2Ni-CNTs. Except for  $\text{H}_2\text{S}$  adsorption, electrons transfer from Ni-CNTs to gas molecules in the adsorption process as Ni atoms act as the electron donor. The large adsorption energy for all of the gas molecules shows that Ni-doped CNTs are an effective gas-sensing material to detect the  $\text{SF}_6$  decomposition components.

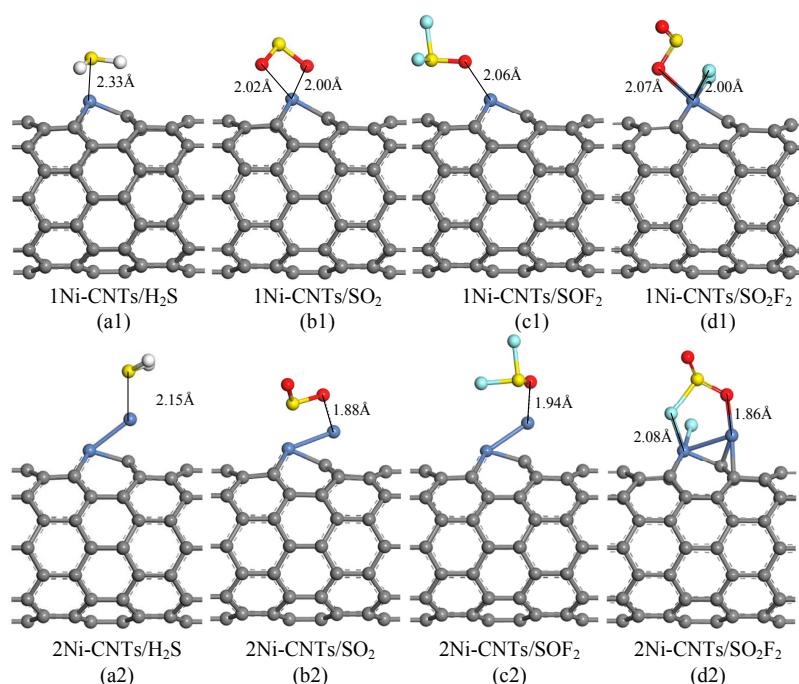


**Figure 6.** Optimized geometries of  $\text{SF}_6$  decomposition components adsorbed Ni-doped CNTs, distances in Å.

**Table 2.** Interaction distance ( $d$ ), adsorption energy  $E_{\text{ads}}$ , charge transfer  $Q_t$  of  $\text{SF}_6$  decomposition components adsorbed Ni-doped CNTs.

System	$d$ (Å)	$Q_t$ (e)	$E_{\text{ads}}$ (eV)
1Ni-CNTs/ $\text{H}_2\text{S}$	2.33	0.25	−0.81
1Ni-CNTs/ $\text{SO}_2$	2.00	−0.35	−1.13
1Ni-CNTs/ $\text{SOF}_2$	2.06	−0.06	−0.49
1Ni-CNTs/ $\text{SO}_2\text{F}_2$	2.07	−0.94	−1.93
2Ni-CNTs/ $\text{H}_2\text{S}$	2.15	0.19	−3.05
2Ni-CNTs/ $\text{SO}_2$	1.88	−0.30	−2.26
2Ni-CNTs/ $\text{SOF}_2$	1.94	−0.26	−2.83
2Ni-CNTs/ $\text{SO}_2\text{F}_2$	1.86	−0.98	0.97

Generally, gas sensors detect the concentration of contacted gas by measuring the change of conductivity during the adsorption process. Density of states (DOS) is one of the effective ways to analyze the change of conductivity upon  $\text{SO}_2$ ,  $\text{H}_2\text{S}$ ,  $\text{SOF}_2$ , and  $\text{SO}_2\text{F}_2$  adsorption. As shown in Figure 7, the DOS around Fermi level for  $\text{H}_2\text{S}$ ,  $\text{H}_2\text{S}$ , and  $\text{SOF}_2$  adsorptions obviously increase in different

degrees, which leads to the corresponding change of conductivity. The change of conductivity has just verified that the Ni-CNT sensor shows a high gas response to  $\text{H}_2\text{S}$ ,  $\text{H}_2\text{S}$ , and  $\text{SOF}_2$ . Meanwhile, the inconspicuous change of DOS upon  $\text{SO}_2\text{F}_2$  adsorption slightly increases the conductivity of the adsorption system, which is consistent with the experimental study.

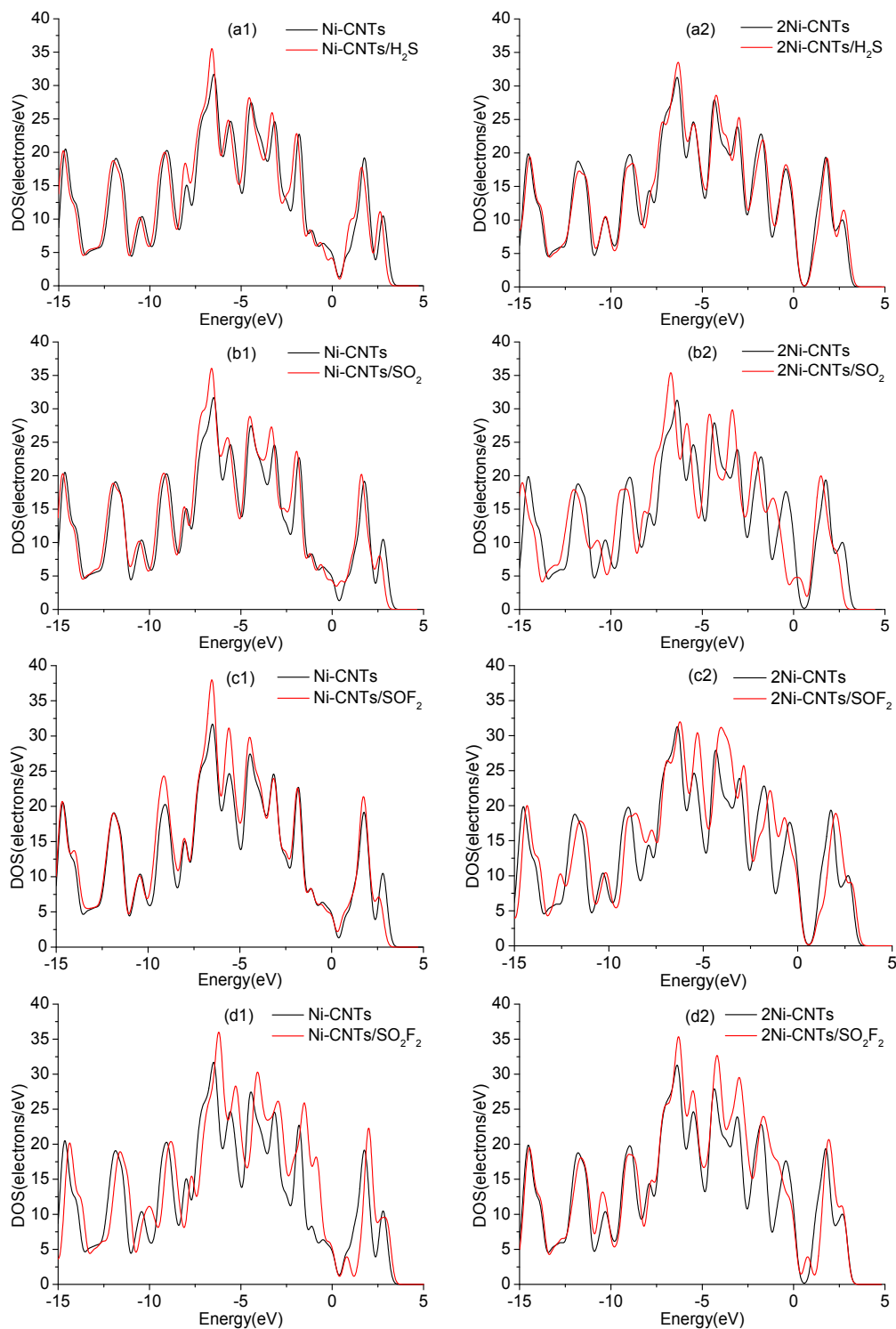


**Figure 7.** Density of states (DOS) of Ni-CNTs, 2Ni-CNTs, and gas adsorbed Ni-CNTs: (a1–d1) represent gas adsorption on Ni-CNTs, (a2–d2) represent gas adsorption on 2Ni-CNTs.

In DOS analysis, the change of conductivity upon H<sub>2</sub>S adsorption is less than SO<sub>2</sub>, SOF<sub>2</sub>, and SO<sub>2</sub>F<sub>2</sub> adsorption, based on the calculation condition that the default temperature is 0 K. However, the detection temperature has increased to ambient temperature, which distinctly enhances the reaction activity of the S atom. In addition, S in H<sub>2</sub>S is much more active than that in SO<sub>2</sub>, SOF<sub>2</sub>, and SO<sub>2</sub>F<sub>2</sub> because it only builds two monovalences with H atoms. As a result, the change of conductivity for a single H<sub>2</sub>S molecule is the largest among four gas molecule adsorptions in the experiment.

#### 4. Conclusions

This study introduces Ni modification on the CNT surface for the sensitive and selective detection of SF<sub>6</sub> decomposition components: SO<sub>2</sub>, H<sub>2</sub>S, SOF<sub>2</sub>, and SO<sub>2</sub>F<sub>2</sub>. The TEM results show that Ni particles evenly distribute on the surface of CNTs. The prepared Ni-CNT gas sensor shows high gas sensitivity as its LOD reaches 1 ppm to SF<sub>6</sub> decomposition components. The sensitivity of the Ni-CNT gas sensor is placed in the following order: H<sub>2</sub>S > SOF<sub>2</sub> > SO<sub>2</sub> > SO<sub>2</sub>F<sub>2</sub>. In addition, the Ni-CNT gas sensor shows good gas-sensing recovery property, which makes it easy to be widely used. DFT theoretical study results verify that conductivity of the adsorption system significantly changes when SF<sub>6</sub> decomposition components interact with Ni-CNTs. Thus, our finding is certainly beneficial to broaden the perspective of Ni-CNT gas sensor applications in evaluating and diagnosing the insulation status of SF<sub>6</sub>-insulated equipment online.

**Author Contributions:** Y.G. and X.Z. proposed the project and analyzed the simulation results. Y.G. contributed to the experimental detection. C.T. and Q.Z. did DFT simulations. P.L. and S.W. did the analysis of the data and gave some revision of the manuscript. All authors read and approved the final manuscript.

**Funding:** This study was supported by the National Key R&D Program of China (Grant No. 2017YFB0902700, 2017YBF0902702), and the Fundamental Research Funds for the Central Universities (Grant No. SWU118030).

**Conflicts of Interest:** The authors declare no conflict of interest.

#### References

1. Tang, J.; Xu, Z.R.; Zhang, X.X.; Sun, C.X. GIS partial discharge quantitative measurements using UHF microstrip antenna sensors. In Proceedings of the 2007 Annual Report—Conference on Electrical Insulation and Dielectric Phenomena, Vancouver, BC, Canada, 14–17 October 2007.
2. Völcker, O.; Koch, H. Insulation co-ordination for gas-insulated transmission lines (GIL). *IEEE Trans. Power Delivery* **2000**, *16*, 122–130. [[CrossRef](#)]
3. Liu, J.; Huang, G.M.; Ma, Z. A Novel intelligent high voltage SF<sub>6</sub> circuit breaker. In Proceedings of the IEEE PES General Meeting, Providence, RI, USA, 25–29 July 2010.
4. Van Brunt, R.J. Production Rates for Oxyfluorides SOF<sub>2</sub>, SO<sub>2</sub>F<sub>2</sub>, and SOF<sub>4</sub> in SF<sub>6</sub> Corona Discharges. Available online: <https://nvlpubs.nist.gov/nistpubs/jres/090/3/V90-3.pdf#page=13> (accessed on 13 October 2018).
5. Walters, J.P. Spark discharge: Application multielement spectrochemical analysis. *Science* **1977**, *198*, 787–797. [[CrossRef](#)] [[PubMed](#)]
6. Sauers, I. By-product formation in spark breakdown of SF<sub>6</sub>/O<sub>2</sub> mixtures. *Plasma Chem. Plasma Process.* **1988**, *8*, 247–262. [[CrossRef](#)]
7. Zhang, X.; Gui, Y.; Dai, Z. A simulation of Pd-doped SWCNT used to detect SF<sub>6</sub> decomposition components under partial discharge. *Appl. Surf. Sci.* **2014**, *315*, 196–202. [[CrossRef](#)]
8. Zeng, F.; Ju, T.; Zhang, X.; Pan, J. Influence regularity of trace H<sub>2</sub>O on SF<sub>6</sub> decomposition characteristics under partial discharge of needle-plate electrode. *IEEE Trans. Dielectr. Electr. Insul.* **2015**, *22*, 287–295. [[CrossRef](#)]
9. Judd, M.D.; Yang, L.; Hunter, I.B.B. Partial discharge monitoring of power transformers using UHF sensors. Part I: sensors and signal interpretation. *IEEE Electr. Insul. Mag.* **2005**, *21*, 5–14. [[CrossRef](#)]
10. Judd, M.D.; Yang, L.; Hunter, I.B.B. Partial discharge monitoring for power transformer using UHF sensors. Part 2: field experience. *IEEE Electr. Insul. Mag.* **2005**, *21*, 5–13. [[CrossRef](#)]

11. Jennings, E.; Collinson, A. A partial discharge monitor for the measurement of partial discharges in a high voltage plant by the transient earth voltage technique. In Proceedings of the 1993 International Conference on Partial Discharge, Canterbury, UK, 28–30 September 1993.
12. Kweon, D.J.; Chin, S.B.; Kwak, H.R.; Kim, J.C. The analysis of ultrasonic signals by partial discharge and noise from the transformer. *IEEE Trans. Power Delivery* **2005**, *20*, 1976–1983. [[CrossRef](#)]
13. Tang, J.; Liu, F.; Zhang, X.X.; Meng, Q.H.; Zhou, J.B. Partial discharge recognition through an analysis of SF<sub>6</sub> decomposition products part 1: Decomposition characteristics of SF<sub>6</sub> under four different partial discharges. *IEEE Trans. Dielectr. Electr. Insul.* **2012**, *19*, 29–36. [[CrossRef](#)]
14. Ding, W.D.; Hayashi, R.; Suehiro, J.; Zhou, G.; Imasaka, K.; Hara, M. Calibration methods of carbon nanotube gas sensor for partial discharge detection in SF<sub>6</sub>/sub 6. *IEEE Trans. Dielectr. Electr. Insul.* **2006**, *13*, 353–361. [[CrossRef](#)]
15. Minagawa, T.; Kawada, M.; Yamauchi, S.; Kamei, M.; Nishida, C. Development of SF<sub>6</sub> decomposition gas sensor. *Surf. Coat. Technol.* **2003**, *169*, 643–645. [[CrossRef](#)]
16. Hanabusa, K.; Takata, S.; Fujisaki, M.; Nomura, Y.; Suzuki, M. Fluorescent gelators for detection of explosives. *Bull. Chem. Soc. Jpn.* **2016**, *89*, 1391–1401. [[CrossRef](#)]
17. Besteman, K.; Lee, J.O.; Wiertz, F.G.M.; Heering, H.A.; Dekker, C. Enzyme-coated carbon nanotubes as single-molecule biosensors. *Nano Lett.* **2003**, *3*, 727–730. [[CrossRef](#)]
18. Qi, P.; Vermesh, O.; Grecu, M.; Javey, A.; Wang, Q.; Dai, H.; Peng, S.; Cho, K.J. Toward large arrays of multiplex functionalized carbon nanotube sensors for highly sensitive and selective molecular detection. *Nano Lett.* **2003**, *3*, 347–351. [[CrossRef](#)]
19. Jing, L.; Lu, Y.; Ye, Q.; Cinke, M.; Han, J.; Meyyappan, M. Carbon nanotube sensors for gas and organic vapor detection. *Nano Lett.* **2003**, *3*, 929–933.
20. Komiyama, M.; Mori, T.; Ariga, K. Molecular imprinting: Materials nanoarchitectonics with molecular information. *Bull. Chem. Soc. Jpn.* **2018**, *91*, 1075–1111. [[CrossRef](#)]
21. Osica, I.; Imamura, G.; Shiba, K.; Ji, Q.; Shrestha, L.K.; Hill, J.P.; Kurzydłowski, K.J.; Yoshikawa, G.; Ariga, K. Highly Networked Capsular Silica-Porphyrin Hybrid Nanostructures as Efficient Materials for Acetone Vapor Sensing. *ACS Appl. Mater. Interfaces* **2017**, *9*, 9945–9954. [[CrossRef](#)] [[PubMed](#)]
22. Zhang, Y.; Yuan, S.; Day, G.; Wang, X.; Yang, X.; Zhou, H.C. Luminescent sensors based on metal-organic frameworks. *Coord. Chem. Rev.* **2018**, *354*, 28–45. [[CrossRef](#)]
23. Chopra, S.; Mcguire, K.; Gothard, N.; Rao, A.M.; Pham, A. Selective gas detection using a carbon nanotube sensor. *Appl. Phys. Lett.* **2003**, *83*, 2280–2282. [[CrossRef](#)]
24. Penza, M.; Rossi, R.; Alvisi, M.; Cassano, G.; Signore, M.A.; Serra, E.; Giorgi, R. Pt-and Pd-nanoclusters functionalized carbon nanotubes networked films for sub-ppm gas sensors. *Sens. Actuators, B chem.* **2008**, *135*, 289–297. [[CrossRef](#)]
25. Tang, J.; Rao, X.; Zeng, F.; Cai, W.; Cheng, L.; Zhang, C. Influence mechanisms of trace H<sub>2</sub>O on the generating process of SF<sub>6</sub> spark discharge decomposition components. *Plasma Chem. Plasma Process.* **2017**, *37*, 1–16. [[CrossRef](#)]
26. Zhang, X.; Chen, Q.; Hu, W.; Zhang, J. A DFT study of SF<sub>6</sub> decomposed gas adsorption on an anatase (101) surface. *Appl. Surf. Sci.* **2013**, *286*, 47–53. [[CrossRef](#)]
27. Zhang, X.; Chen, Q.; Tang, J.; Hu, W.; Zhang, J. Adsorption of SF<sub>6</sub> decomposed gas on anatase (101) and (001) surfaces with oxygen defect: A density functional theory study. *Sci. Rep.* **2014**, *4*, 4762. [[CrossRef](#)] [[PubMed](#)]
28. Zhang, X.; Yu, L.; Wu, X.; Hu, W. Experimental sensing and density functional theory study of H<sub>2</sub>S and SOF<sub>2</sub> adsorption on Au-modified graphene. *Adv. Sci.* **2015**, *2*, 1500101. [[CrossRef](#)] [[PubMed](#)]
29. Zhang, X.; Dong, X.; Gui, Y. Theoretical and experimental study on competitive adsorption of SF<sub>6</sub> decomposed components on Au-modified anatase (101) surface. *Appl. Surf. Sci.* **2016**, *387*, 437–445. [[CrossRef](#)]
30. Zhang, X.; Luo, C.; Tang, J. Sensitivity characteristic analysis of adsorbent-mixed carbon nanotube sensors for the detection of SF<sub>6</sub> decomposition products under PD conditions. *Sensors* **2013**, *13*, 15209. [[CrossRef](#)] [[PubMed](#)]

31. Star, A.; Joshi, V.; Skarupo, S.; Thomas, D.; Gabriel, J.C.P. Gas sensor array based on metal-decorated carbon Nanotubes. *J. Phys. Chem. B* **2006**, *110*, 21014–21020. [[CrossRef](#)] [[PubMed](#)]
32. Zhang, X.; Tie, J.; Zhang, J. A Pt-doped TiO<sub>2</sub> nanotube arrays sensor for detecting SF<sub>6</sub> decomposition products. *Sensors* **2013**, *13*, 14764. [[CrossRef](#)] [[PubMed](#)]



© 2018 by the authors. Licensee MDPI, Basel, Switzerland. This article is an open access article distributed under the terms and conditions of the Creative Commons Attribution (CC BY) license (<http://creativecommons.org/licenses/by/4.0/>).